J Physiol Sci (2016) 66:463–476
DOI 10.1007/s12576-016-0441-8

ORIGINAL PAPER

Electrophysiology, immunophenotype, and gene expression characterization of senescent and cryopreserved human amniotic fluid stem cells

Florin Iordache[1] · Andrei Constantinescu[1] · Eugen Andrei[1] · Bogdan Amuzescu[2] · Ferdinand Halitzchi[2] · Lorand Savu[3] · Horia Maniu[1]

Received: 22 September 2015 / Accepted: 12 February 2016 / Published online: 6 April 2016

Abstract We characterized human amniotic fluid stem cells (AFSC) in senescent cultures (6 weeks) versus cryopreserved cells using whole-cell patch-clamp, immunophenotyping, and differential gene expression profiling for senescence genes. We evidenced five ion current components (outward rectifier, A-type, inward rectifier, and big conductance Ca^{2+}-dependent K^+ currents, fast voltage-dependent Na^+ currents). Senescent AFSC showed reduced expression of CD90, CD44, CD133, over 500-fold increase of interferon gamma and telomerase reverse transcriptase genes, increased cycle-dependent kinase 4 inhibitors, p53-binding protein 1, and decreased calreticulin and CD44. HLA-ABC immune expression was similar, and HLA-DR expression very low in both cell types. A subset of cryopreserved AFSC featured large inward rectifier K^+ currents, voltage-dependent Na^+ currents, and neural progenitor markers evidenced by immunophenotyping and RT-PCR. In all AFSC, in both culture conditions, at patch rupture the outward currents were very low, and they increased progressively over several minutes upon cytoplasm dialysis with pipette solution.

F. Iordache and A. Constantinescu contributed equally to this work.

✉ Bogdan Amuzescu
bogdan@biologie.kappa.ro

[1] Flow Cytometry and Cell Therapy Laboratory, "N. Simionescu" Institute of Cellular Biology and Pathology, B.P. Hasdeu Str. 8, 050568 Bucharest, Romania

[2] Department Biophysics and Physiology, Faculty of Biology, University of Bucharest, Splaiul Independentei 91-95, 050095 Bucharest, Romania

[3] Genetic Lab SRL, Cpt. Av. N. Drossu Str. 9, 012071 Bucharest, Romania

Keywords Amniotic fluid stem cell · Cryopreserved cell · Differential gene expression · Immunophenotype · Patch-clamp · RT-PCR

Abbreviations

2-APB	2-aminoethyl diphenylborinate
4-AP	4-aminopyridine
AF	Amniotic fluid
AFSC	Amniotic fluid stem cells
AKT	Serine/threonine-specific protein kinase, protein kinase B (PKB)
ANOVA	Analysis of variance
bFGF	Basic fibroblast growth factor (FGF-2 or FGF-β)
BK or BK(Ca)	Big conductance Ca^{2+}-dependent K^+ channels
BM-MSC	Bone marrow-derived mesenchymal stem cells
BMP-4	Bone morphogenetic factor 4
CACN	Voltage-dependent Ca^{2+} channel subunit gene
CALR	Calreticulin
CD	Cluster of differentiation
CDK	Cycle-dependent kinase
CFU-F	Colony forming unit—fibroblastic
c-Kit	Tyrosine protein kinase encoded by KIT gene, SCFR
DAPI	2-(4-amidinophenyl)-1*H*-indole-6-carboxamidine
DMSO	Dimethylsulfoxide
DR	D-related, delayed rectifier
E	Epithelioid
EGTA	Ethylene glycol tetraacetic acid
ERK	Extracellular signal-regulated kinases
ESC	Embryonic stem cell

F	Fibroblastic
FACS	Fluorescence-activated cell sorting
FITC	Fluorescein isothiocyanate
GIRK	G-protein-coupled inward rectifying K^+ channel
HCAM	Human cell adhesion molecule
HCN	Hyperpolarization-activated cyclic nucleotide-gated channel gene
hEAG	Human ether-à-go–go related gene
HLA	Human leukocyte antigen
IFNG	Interferon gamma gene
IGFBP2 and 3	Insulin-like growth factor-binding proteins 2 and 3
Ipsc	Induced pluripotent stem cell
IR	Inward rectifier
Jak/Stat	Janus kinase/Signal transducer and activator of transcription (pathway)
KCN	Voltage-dependent K^+ channel gene
Klf4	Kruppel-like factor 4
K-Ras	Kirsten rat sarcoma viral oncogene homolog GTPase
LIF	Leukemia inhibiting factor
MAPK	Mitogen-activated protein kinases
MEK	Mitogen-activated protein kinase kinase, MAPK
MHC	Major histocompatibility complex
MSC	Mesenchymal stem cells
Nanog	Name chosen by Prof. Ian Chambers (Univ. Edinburgh) after the Tír na nÓg legend
NMDG	*N*-methyl D-glucamine
Oct-3	Octamer-binding transcription factor 3
PBS	Phosphate buffered saline
PBS-T	PBS with Triton X-100
PE	Phycoerythrin
PI(3)K	Phosphoinositide 3-kinase
PIP_2	Phosphatidylinositol (4,5) bisphosphate
RAF	Family of serine/threonine protein kinases related to retroviral oncogenes that enhance fibrosarcoma induction, participating in the MAPK (RAS-RAF-MEK-ERK) signaling cascade
RNA	Ribonucleic acid
RT-PCR	Reverse-transcription polymerase chain reaction
RuR	Ruthenium red
SCFR	Mast/stem cell growth factor receptor
SCN	Voltage-dependent Na^+ channel gene
SD	Standard deviation
SEM	Standard error of the means
SMAD	Homologs of *Drosophila* protein Mothers Against Decapentaplegic (MAD) and *C. elegans* protein SMA (small body size)
Sox-2	SRY(sex determining region Y)-box 2
SSEA	Stage-specific embryonic antigen
Tbx3	T-box 3
TEA	Tetraethylammonium
TERT	Telomerase reverse transcriptase gene
TGF-β	Transforming growth factor beta
Thy-1	Thymocyte differentiation antigen 1
TIMP-1	Tissue inhibitor of metalloproteinase 1
TP53BP1	Tumor suppressor p53 binding protein 1
Tra	Tumor-rejection antigen
TRPM	Transient receptor potential, melastatin-related ion channel
Upa	Urinary plasminogen activator
VEGF	Vascular endothelial growth factor

Introduction

Mesenchymal stem cells (MSC) have recently been the focus of intensive research due to encouraging results in both in vitro experiments and clinical trials, and the promise to revolutionize the therapy and outcome in a variety of pathologies, including traumatic or ischemic injury of the central or peripheral nervous system [1], myocardial infarction [2], cancer therapy [3], as well as regenerative medicine approaches for various tissues and organs [4, 5]. Given the large variety of protocols for isolation, expansion, and characterization, a minimal definition of MSC could include "stromal" origin, fibroblast-like spindle-shape morphology, adherence to plastic culture dishes, capacity of proliferation and colony formation (the fibroblast colony forming unit—CFU-F—assay is still considered the "golden standard" for MSC identification), and potential to multiple differentiation into mesoderm derivatives in appropriate culture conditions, comprising at least trilinear differentiation: adipocytes, chondroblasts, and osteoblasts, evidenced with oil red O, alcian blue, and alizarin red S staining, respectively [6]. MSC can be isolated from a broad range of tissues, including bone marrow, peripheral blood, menstrual fluid, deciduous teeth dental pulp, synovial fluid and membrane, adipose tissue, umbilical cord blood, Wharton's jelly, fetal liver, placenta, and amniotic fluid (AF). The latter is a convenient source due to the ease of harvesting mesenchymal cells from AF collected during the second trimester of pregnancy via amniocentesis under ultrasonographic guidance, a routine prenatal screening procedure, far less invasive than bone marrow aspiration puncture/biopsy [7].

AF is an abundant source of cells with multiple origins, including skin and digestive tract of the developing embryo or fetus, but also MSC derived from the amniotic

membrane [8]. Based on morphology and proliferation potential, multiple subpopulations of viable adherent AF cells have been described, including epithelioid (E-type: 33.7 %), AF-specific (AF-type: 60.8 %), and fibroblastic (F-type: 5.5 %) cells [9, 10]. In appropriate culture conditions, a stem cell population (AFSC) can be expanded, expressing markers specific for pluripotent undifferentiated embryonic stem cells (ESC) like Oct4 (Pou5f1), Sox2, Wdr5, Klf4, Nanog, pluripotency surface antigens SSEA1, SSEA3, SSEA4 (stage-specific embryonic antigens), Tra-1-60 and Tra-1-81 (tumor-rejection antigens) [11], mesenchymal markers like CD73 (5′-nucleotidase), CD90 (Thy-1, thymocyte antigen 1) and CD105 (endoglin, part of the TGFβ receptor complex), receptors for adhesion molecules like CD29 (integrin β1, fibronectin receptor) and CD44 (HCAM—homing cell adhesion molecule, hyaluronic acid receptor), CD166, class I HLA receptors (MHC-I), and being substantially negative for hematopoietic and endothelial markers like CD11b, CD14, CD34, CD45, CD133, CD31, and MHC class II antigens like HLA-DR [8, 9, 12]. The pioneering studies of De Coppi et al. have defined conditions for AFSC differentiation into a variety of tissues, including adipose tissue, bone, skeletal muscle, endothelium, nervous tissue, and liver [13]. Culture and differentiation protocols were based on either non-sorted AFSC populations or selected populations using magnetic microbeads or flow cytometry methods (FACS—fluorescence-activated cell sorting), most often according to the presence/absence of marker CD117 (c-Kit, mast/stem cell growth factor receptor—SCFR). Recent studies have shown that both c-Kit positive and negative AFSC are capable of multipotent differentiation, the only remarkable difference being an enhanced myocardial differentiation propensity in c-Kit positive cells, rendering them suitable for cardiac regenerative therapies [14].

AFSC exert their therapeutic attractiveness due to a number of favorable features and qualities, including ease of obtaining, lack of significant bioethics and medical ethics concerns and restrictions, specific for ESC research and applications, capacity of in vitro expansion, lack of immune reactions when administered in vivo due to absence of MHC-II surface antigens and immunosuppressive properties, exploited in treatment of severe autoimmune diseases and wound and scar healing, absence of teratoma or malignant tumor formation, in contrast to ESC, accompanied by lack of karyotypic abnormalities and maintenance of long telomeres despite the high proliferative potential [7, 8, 13]. Recent molecular biology studies have revealed many interesting and peculiar features of pluripotency maintenance in cultured AFSC, related to the complex transcriptional network of Oct4, Sox2, and Nanog, which is modulated by two signaling cascades [12]. One of them, specific to naive pluripotent stem cells, acts via LIF (leukemia inhibiting factor) and BMP4 (bone morphogenetic factor 4) to regulate Nanog expression, comprising LIF-induced activation of PI(3)K/AKT, induced T-box 3 (Tbx3) expression, parallel activation of the Jak/Stat3 pathway to induce Klf4 expression and further Nanog expression, and a third pathway including MEK and ERK1/2. The second, more active in primed bFGF-dependent (fibroblast growth factor) pluripotent stem cells, includes activin A/TGFβ receptors acting via SMAD2/3. It has been shown that the human Nanog promoter has independent Tbx3 and SMAD2/3 binding sites [15, 16]. In spite of these impressive achievements, a lot remains to be uncovered and understood about the pluripotency and differentiation properties of AFSC in vitro, including the biological signals that control their evolution and determine their fate, in order to develop novel stem cell therapies based on rational scientific criteria. Therefore the aim of our study was to evidence differentiation or steady-state attained during culturing by assessing the molecular properties of human AFSC in two distinct conditions, senescent versus cryopreserved cells, to render a comprehensive immunophenotype and gene expression profile, and an electrophysiology screening via the whole-cell patch clamp technique.

Materials and methods

Amniotic fluid cell cultures

The amniotic fluid cell cultures were kindly provided by Genetic Lab S.R.L. diagnostics laboratory upon informed consent of the patients in agreement with national and EU rules. The primary cultures were obtained by centrifugation of amniotic fluid at 1050 rpm for 10 min. The cells were then cultured for 10 days without passages at Genetic Lab in AmnioMax medium (Life Technologies Corporation, Carlsbad, CA, USA) supplemented with 10 % fetal bovine serum, 1 % penicillin and 1 % streptomycin and neomycin antibiotics, then delivered to IBPC "N. Simionescu". The senescent cells were obtained by maintaining the cell cultures for 6 weeks in the same conditions (medium changes twice weekly without passages).

Cryopreserved cells were frozen using a cryoconservation medium supplemented with 10 % dimethylsulfoxide (DMSO) either at 10 d.i.v. following harvesting or after a supplementary number of 2–4 weekly passages, kept in liquid nitrogen, then thawed and used for experiments during the subsequent 7 days. Throughout the article, these two different culturing conditions are referred to as "senescent cells" and "cryopreserved cells", respectively.

Electrophysiology

Patch pipettes were prepared from thick-walled borosilicate glass capillaries with inner filament (GC150F-10, Harvard Apparatus Ltd., Edenbridge, UK) via four-stage pulling with a computerized vertical puller (PUL-100, WPI, Sarasota, FL), followed by thermal polishing of the tip by a glass-coated Pt–Ir filament under direct optical control, in order to achieve a resistance of 1–3 MΩ when immersed in solution. Experiments were performed at 22–23 °C on the platform of an inverted microscope (IMT-2, Olympus, Tokyo, JP) equipped with a Peltier temperature controller (TC202A, Harvard Apparatus, Holliston, MA, USA). Currents were converted and processed with a resistive feedback patch-clamp amplifier (WPC-100, ESF electronic, Göttingen, DE), low-pass filtered at 3 kHz with the built-in four-pole Bessel filter, sampled with a Digidata 1322A interface controlled by the Clampex 8.2 module of the pClamp software (Axon Instruments, division of Molecular Devices, Sunnyvale, CA, USA) and stored on a hard-disk for further analysis with the Clampfit module.

Immunofluorescence for neural progenitor markers

Cryopreserved AFSC cultured on 13-mm glass coverslips were washed twice with PBS, fixed for 20 min with paraformaldehyde 4 % in PBS, rewashed twice with PBS, permeabilized with Triton X-100 0.3 % in PBS (PBS-T) for 2 × 15 min, blocked with normal goat serum 4 % in PBS-T (used for all subsequent washing and dilution of antibodies) for 1 h, treated with primary antibodies: tubulin β-III (mouse monoclonal, Abcam ab78078, 1:4000) and neurofilament NF-200 (mouse monoclonal, Sigma N0142, 1:400) vs. negative control (dilution vehicle only) for 3 h at room temperature, washed 3 × 2–3 min, treated with secondary antibody (AlexaFluor® 488 goat anti-mouse, Invitrogen A-11001, 1:1000) for 1 h at room temperature, washed 3 × 2–3 min and 2 × 1 min with purified water, mounted on glass microscopy slides with ProLong® Gold antifade with DAPI (Invitrogen P36935) and examined with an inverted fluorescence microscope.

AFSC immunophenotype profile

The expression of cell surface markers was assessed by flow cytometry (Gallios, Beckman-Coulter) using 1×10^5 cells stained with fluorochrome-conjugated (FITC—Fluorescein-isothiocyanate and PE—Phycoerythrin) primary antibodies against CD29, CD44, CD56, CD90, CD105, CD133, HLA-ABC. and HLA-DR (Dako, Beckman-Coulter), tubulin β-III, neurofilament NF200 (same antibody sets as for immunofluorescence). AFSC were detached using Accutase (Sigma-Aldrich) and washed in phosphate-buffered saline solution (1× PBS). Cells were then incubated with the antibodies at room temperature in the dark for 20 min. For tubulin β-III, neurofilament NF200 the AFSC were permeabilized with 1 ml ice-cold methanol and incubated at −20 °C for 10 min. Furthermore, the cells were centrifuged and washed twice in PBS with 1 % BSA. For negative controls, AFSC were stained with the corresponding isotype-matched IgG antibodies (Dako). Flow cytometry data were analyzed using the Gallios software (Beckman-Coulter).

AFSC gene expression profile

The RNA transcripts were obtained by RNA isolation using the GenElute Mammalian Total RNA Miniprep kit (Sigma-Aldrich), and the cDNA was obtained using the FastLane cell cDNA kit (Qiagen). The isolation and reverse transcription steps were performed according to the manufacturer's specifications. The nucleic acid concentration was determined with a NanoDrop spectrophotometer (Thermo Scientific). Quantitative real-time PCR was performed using the RT^2 Profiler PCR Array Human Cellular Senescence (Qiagen) according to the manufacturer's specifications. PCR reactions were carried out using a ViiA7 thermo-cycler (Applied Biosystems). Data analysis was performed using the web-based RT^2 Profiler PCR Array Data Analysis (Qiagen).

qRT-PCR

To assess the gene expression level for neuroD1 and GIRK2 in cryopreserved AFSC total cellular RNA was isolated from cultured cells using GeneElute Mammalian Total RNA Miniprep Kit (Sigma-Aldrich, St. Louis, MO, USA) and reverse-transcription reaction was performed using M-MLV polymerase (High-Capacity cDNA Reverse Transcription kit (Applied Biosystems, MA, USA). The mRNA levels were quantified by SYBR® Green amplification of cDNA using a real-time thermocycler (ViiA7, Applied Biosystems, USA). Oligonucleotide primers were as follows: neuroD1 forward: CTGCTCAGGACCTACTA ACAACAA and reverse GTCCAGCTTGGAGGACCTT [17]; GIRK2 forward: CCCTCCTGGACTCC'T'T and reverse CCCTCT'GGCATTTATCT [18]; β-actin forward TTGCTGACAGGATGCAGAAG and reverse ACATC TGCTGGAAGGTGGAC. The PCR reaction was optimized starting from the following scheme: denaturation step at 95 °C for 3 min, 40 cycles of denaturation at 95 °C, 15 s, annealing and amplification at 51–56 °C, 45 s, followed by melting curve. The gene expression level was normalized to β-actin. The amplicons were visualized by 2 % agarose gel electrophoresis and ethidium bromide staining.

Solutions and chemicals

The extracellular solution was K^+ Tyrode, with the following composition (in mM): NaCl 135, KCl 5.4, NaH_2PO_4 0.33, HEPES 10, pH 7.40 at 25 °C titrated with NaOH 1 M. $CaCl_2$ 1.8 mM, $MgCl_2$ 0.9 mM and D-glucose 10 mM were freshly added during the day of experiment from 1 M stock solutions. The pipette solution was composed of KCl 140, EGTA 5, HEPES 10, pH 7.21 at 25 °C with KOH. In certain experiments, we used Na^+-free external solution, prepared via Na^+ replacement with *N*-methyl-D-glucamine ($NMDG^+$) at the same concentration. The pharmacological compounds applied were 4-aminopyridine (4-AP) 3 mM, and tetraethylammonium (TEA) 5 mM, freshly prepared from aqueous stock solutions. In addition, we used ruthenium red (RuR) (R2751, Sigma, St Louis, MO, USA) 100 μM, 2-aminoethyl diphenylborinate (2-APB) (D9754, Aldrich, St Louis, MO, USA) 100 μM, and paxilline (P-450, Alomone Labs, Jerusalem, IL, USA) 1 μM, freshly prepared from aqueous stock solutions (RuR) or DMSO stock solutions (2-APB and paxilline). Solutions were delivered to cells via a home-made application system built from an eight-way manifold with G18 syringe needles and an Eppendorf gel-loader, with a flow rate of ~1 ml/min.

Data analysis

Data are expressed as mean ± standard deviation (SD) or mean ± standard error of the means (SEM), as appropriate. In all instances *n* signifies the number of cells analyzed in a certain experimental condition. Statistical analysis was performed using Student's *t* test or Fisher's exact probability test, using a critical level of $p = 0.05$. For immunophenotyping and gene expression profiling, statistical analysis was performed using the one-way ANOVA method for correlated samples.

Results

The general electrical features of the two groups of AFSC (senescent and cryopreserved) approached via whole-cell patch-clamp are listed in Table 1. The access resistance (R_a) was usually below 10 MΩ, and in a majority of cells the seal remained stable over the entire duration of electrophysiology experiments. In both groups of AFSC we found multiple components of voltage-dependent K^+ currents, as illustrated in Fig. 1: an outward rectifying current component showing no inactivation; an A-type (i.e., inactivating) current component with variable sensitivity to 4-AP; current fluctuations, more pronounced at large depolarization steps (+50 and +60 mV), suggestive of big conductance Ca^{2+}-dependent K^+ currents (BK or maxi-K), inhibited reversibly by TEA 5 mM. The inactivation time constant of the A-type current was highly variable, indicating, together with the variable sensitivity to 4-AP, a diversity of molecular species contributing to this inactivatable current component. Average values of the inactivation time constant at +60 mV were 195 ± 378 ms (mean ± SD) in primary senescent AFSC (range between 6.67 and 727.86 ms), and 101 ± 77 ms in cryopreserved AFSC (range: 13.93 and 236.60 ms).

As shown in Fig. 1b, c, activation of these outward current components was progressive: at patch rupture and penetration in the whole-cell configuration the current amplitudes were very low, and they increased gradually over time intervals of several minutes, most likely as a result of the dialysis of cell cytoplasm with pipette solution. A possible explanation of this phenomenon is an effect of calcium release from endoplasmic reticulum intracellular stores upon inositol triphosphate (IP3) receptors activation by the high concentration of calcium buffer (5 mM EGTA) in the pipette solution. This secondary calcium efflux may in turn activate multiple current components. It is known that ion channels lacking intrinsic sensitivity to intracellular calcium may achieve this sensitivity via interaction with calcium-sensitive cytoskeletal proteins. An example is the interaction of inactivating K^+ channels Kv4.2 and 4.3 with neuronal calcium sensor-1 (NCS-1) [19]. Our hypothesis that TRPM7 channels may contribute to the outward rectifier current, upon their activation via intracellular Mg^{2+} binding by EGTA, was rejected by the lack of inhibition of this outward current by either RuR 100 μM or 2-APB 100 μM.

In Fig. 2a we show that paxilline 1 μM in the extracellular solution markedly reduced the current fluctuations at large depolarizations (+50 and +60 mV), proving that they are the result of BK channel activity. Subsequently we analyzed the power density spectra of BK channel fluctuations obtained from currents recorded during the depolarizing step at +60 mV by applying a fast Fourier transform algorithm in Clampfit 10, using a fourth-order Blackman–Harris window function to limit spectral leakage. Spectra were fitted over a relevant interval of frequencies with a Lorentz power function, as shown in Fig. 2b:

$$S(f) = \sum_{i=1}^{n} \frac{S(0)_i}{1 + (f/f_{ci})^2}$$

where $S(f)$ is the spectral power density at frequency f, $S(0)$ the plateau power density, and f_c the angular or corner frequency. Given the well-known relationship:

$$2\pi f_c = k_{op} + k_{cl}$$

Table 1 General electrical properties of the two groups of AFSC approached via whole-cell patch-clamp

Feature	R_p (MΩ)	C_m (pF)	R_m (MΩ)	R_a (MΩ)	τ (μs)	I_{hold} (pA)	Preservation of the seal at the end of exp.
Senescent AFSC ($n = 18$)							
Mean	2.03	47.27	2021.34	7.62	370.55	−179.17	72.22 %
SD	0.83	22.28	2253.96	4.44	291.41	295.54	
Cryopreserved AFSC ($n = 19$)							
Mean	2.33	44.97	1519.67	8.92	415.46	−100.95	78.94 %
SD	0.77	26.75	1927.00	4.24	330.09	95.71	

R_p pipette resistance, C_m membrane capacitance, R_m membrane resistance, R_a access resistance, τ time constant of the equivalent electrical circuit, I_{hold} holding current at −80 mV

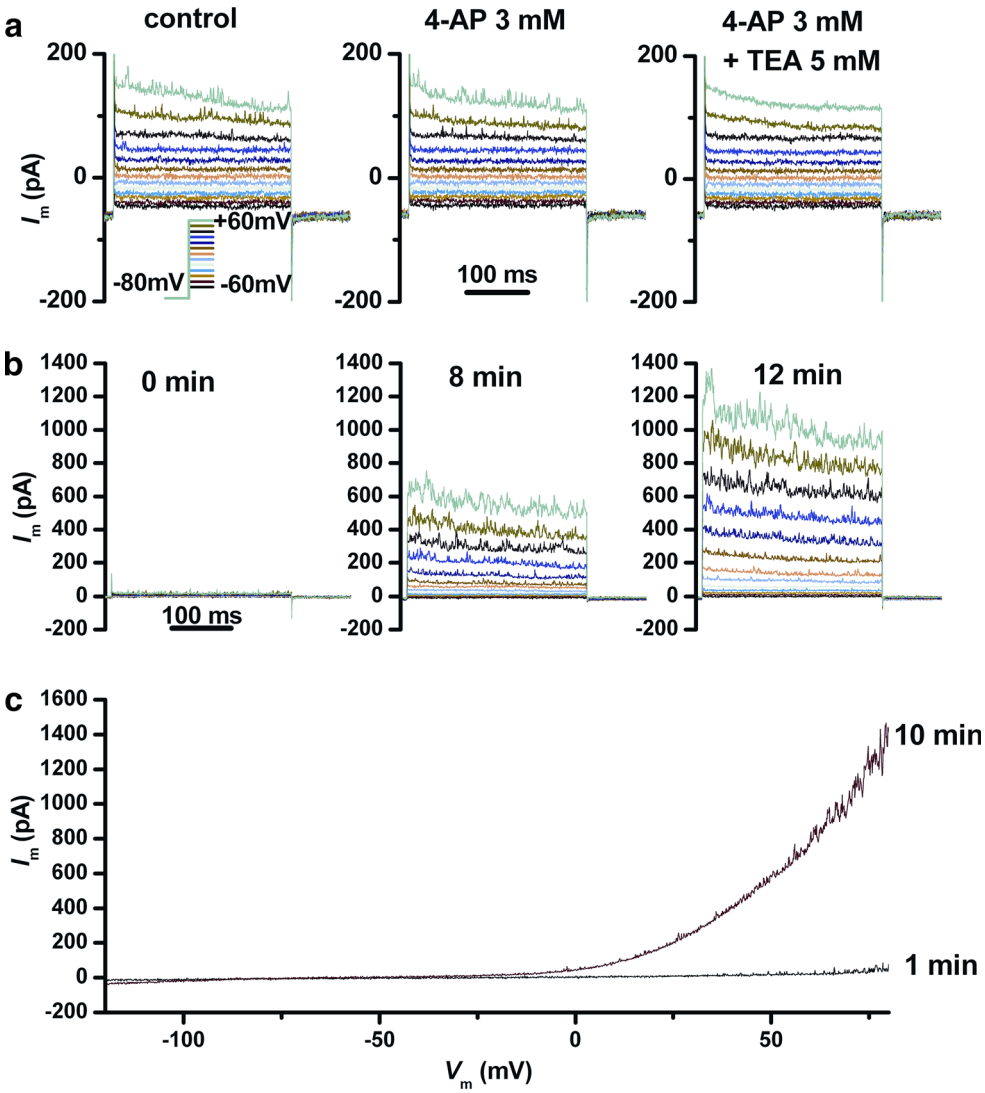

Fig. 1 Outward currents elicited by depolarizing voltage pulses in a senescent AFSC. **a** A combination of outward rectifier and A-type currents, and current fluctuations suggestive of BK $K^+(Ca^{2+})$ channels. Application of 4-AP modified the time constant of inactivation, and addition of TEA reversibly inhibited the current fluctuations. **b** Gradual development of outward currents at different times after penetration in the whole-cell configuration (same voltage protocol as in **a**). **c** Gradual development of outward currents evidenced using voltage ramps from −120 to +80 mV at 1 and 10 min after patch rupture

an estimation of the corner frequency allows an estimation of the opening and closing rates (k_{op} and k_{cl}) of the channels producing the fluctuations in the frame of a simplified two-state open-closed gating model [20]. The values obtained in our study were: $S(0) = 0.96 \pm 2.14$ pA^2/Hz (mean ± SD, $n = 22$) and $f_c = 288 \pm 137$ Hz for senescent AFSC, and $S(0) = 52 \pm 105$ pA^2/Hz (mean ± SD, $n = 23$) and $f_c = 169 \pm 189$ Hz for cryopreserved AFSC.

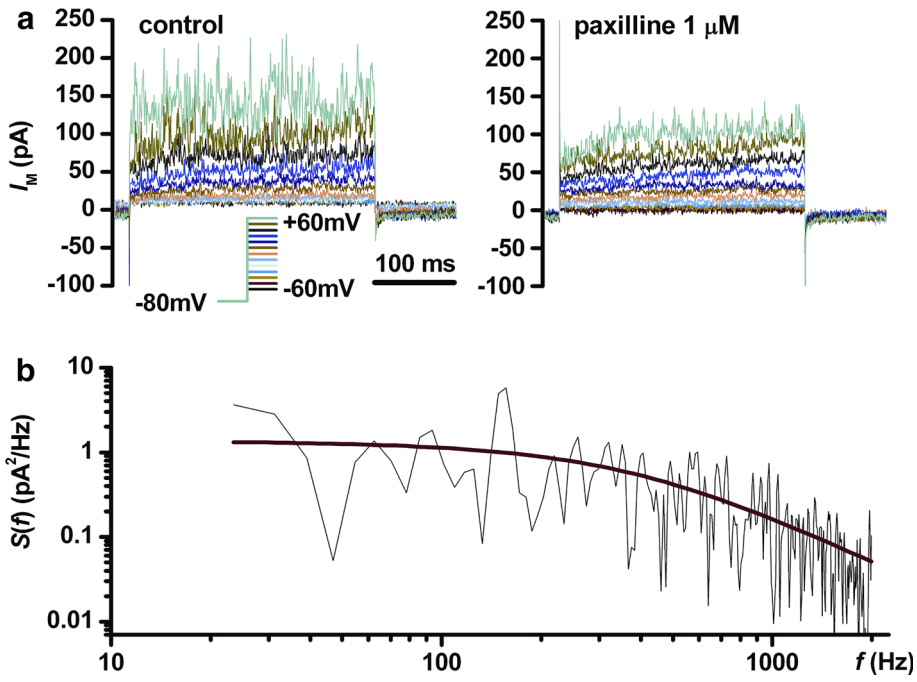

Fig. 2 Analysis of BK-like current fluctuations. **a** Voltage-clamp recordings in a cryopreserved AFSC in control conditions and after application of paxilline 1 μM in the external solution. **b** Fourier transform of the current trace at +60 mV in control conditions shown in **a**, fitted with a Lorentz function

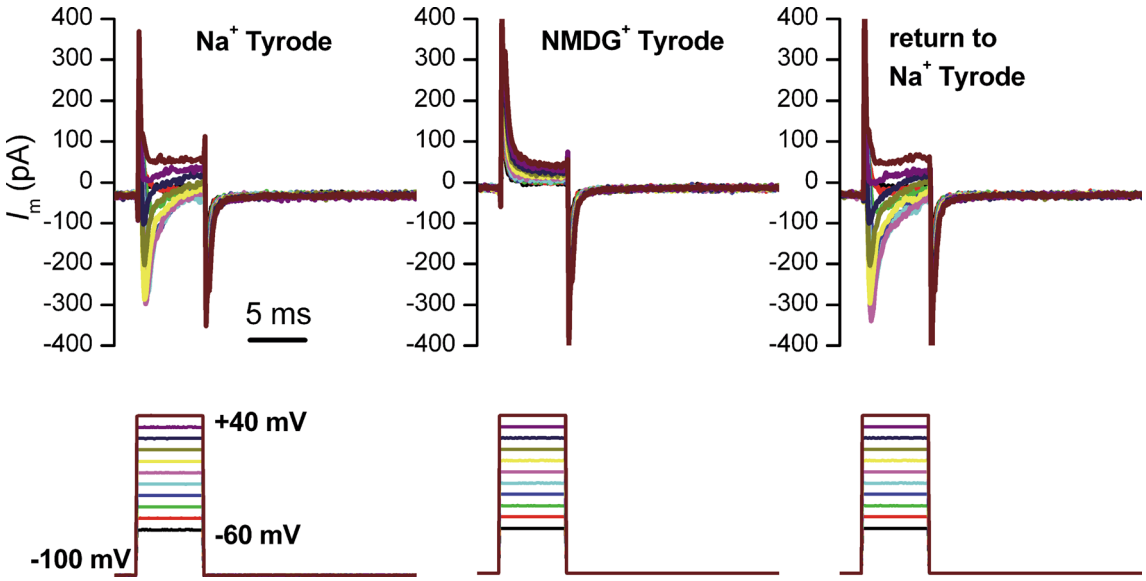

Fig. 3 Voltage-dependent Na^+ current in a senescent AFSC, and its reversible disappearance upon Na^+ replacement with the impermeant organic cation $NMDG^+$ in the external solution

In large numbers of cells from both experimental groups we detected voltage-dependent Na^+ currents, with maximum peak amplitude at −10 or 0 mV depolarizing steps. Na^+ replacement in the external Tyrode solution with an impermeant organic cation, *N*-methyl-D-glucamine ($NMDG^+$), resulted in a reversible disappearance of the inward current. A typical experiment is shown in Fig. 3. This simple approach confirms the nature of the current—voltage-dependent Na^+ current—excluding other inward currents via voltage-dependent Ca^{2+} channels.

In Fig. 4 we present an interesting cellular phenotype, suggestive for neuronal differentiation, found in five cryopreserved AFSC, consisting in high densities of voltage-dependent Na^+ current (individual peak amplitude values: 9.2, 9.6, 18.5, 84.7, 21.7 pA/pF) and appearance of an inward rectifying K^+ current (individual values at −120 mV: 3.8, 4.4, 5.8, 65.8, 18.9 pA/pF). The inward rectifier current disappeared upon K^+ substitution with Cs^+ in the Tyrode solution, and was partly inhibited by RuR 100 μM (Fig. 4d).

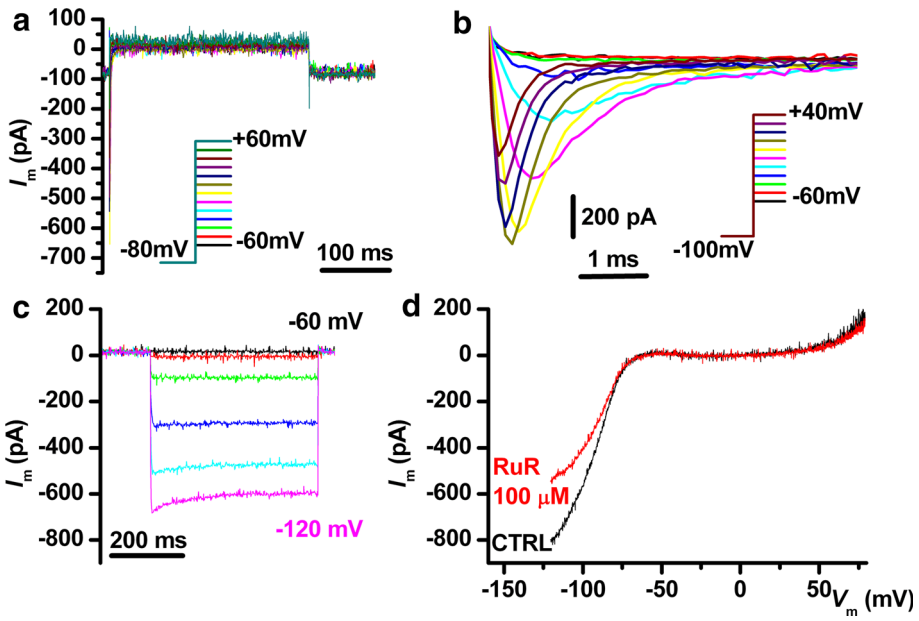

Fig. 4 Electrical phenotype of a cryopreserved AFSC suggestive of neuronal differentiation. **a** Absence of outward rectifying currents. **b** Large voltage-dependent Na^+ currents. **c** Large inward rectifying K^+ currents elicited by hyperpolarizing steps from −60 to −120 mV from a holding potential of −60 mV. **d** I–V plot of the inward rectifying current shown in **c** and its partial inhibition by RuR 100 µM

We also searched for supplementary evidence of neuronal/glial progenitor commitment in cryopreserved AFSC, to confirm electrophysiology findings. Thus, using indirect immunofluorescence we found intense staining for tubulin β-III and considerably weaker staining in a subset of cells for heavy subunit neurofilaments (200 kDa, NF-200) (Fig. 5a). Via flow cytometry three neural markers were found positive: tubulin β-III, NF-200, and CD56/NCAM (Fig. 5b), while RT-PCR followed by agarose gel electrophoresis and ethidium bromide staining revealed expression of neuronal precursor markers NeuroD1 and a variant of the inward rectifier K^+ channel gene transcript, GIRK2; SYBR® Green quantitation showed moderate levels of expression relative to a reference gene, β-actin (Fig. 5c).

In Table 2 we summarized the experimental data comprised of average current densities, numbers, and percentages of cells expressing different current components in the two experimental groups. We found marked differences between these groups for the A-type inactivating outward rectifier current (I_A) ($p = 0.0247$, one-tailed Fisher's exact test), expressed in a larger proportion of senescent AFSC, and for the inward rectifier K^+ current (I_{Kir}) ($p = 0.0523$), present almost exclusively in cryopreserved AFSC, together with higher densities of I_{Na}. Generally current densities tended to be larger in cryopreserved AFSC.

The immunophenotype characterization of senescent vs. cryopreserved AFSC (Fig. 6) revealed statistically significant decreases in surface density of MSC markers CD90 (Thy-1 antigen), CD44 (HCAM, hyaluronic acid receptor), and hematopoietic, endothelial, neuronal and glial stem cell marker CD133 (Prominin 1). The differential gene expression profile (Fig. 7a, b) shows a marked over-expression (over 500-fold increase) in senescent AFSC cultures of interferon γ (IFNG) and telomerase reverse transcriptase (TERT), as well as milder increases in expression of inhibitors of CDK4 kinase (CDKN2A, CDKN2D), tumor suppressor p53 binding protein 1 (TP53BP1), and an under-expression of calreticulin (CALR) and CD44, confirming the immunophenotype results for this marker.

Discussion

Using a powerful combination of biophysical and molecular biology methods we have succeeded to unravel the dominant electrophysiology, immunophenotype and gene expression features of human AFSC cultured in controlled medium conditions, and to evidence specific changes in expression induced in senescent cultures, at over 6 weeks in vitro.

To date there is a paucity of studies approaching the electrophysiology of various stem cell populations and preparations. An important contribution in this field has been brought by the reports of a group at the Research Centre on Heart, Brain, Hormones, and Healthy Aging, Faculty of Medicine, University of Hong-Kong. Using a combination of whole-cell patch-clamp recordings and RT-PCR, they demonstrated the presence in rat bone marrow-derived MSC (BM-MSC) of multiple ion current components, including TTX-sensitive voltage-dependent Na^+ channels (the human neuroendocrine-specific isoform hNE-Na) (I_{Na}), nifedipine-sensitive L-type Ca^{2+} channels (I_{CaL}), 4-AP-sensitive fast (Kv4.2 and 4.3) and slow (Kv1.4) transient outward K^+ channels ($I_{to\ fast\ \&\ slow}$),

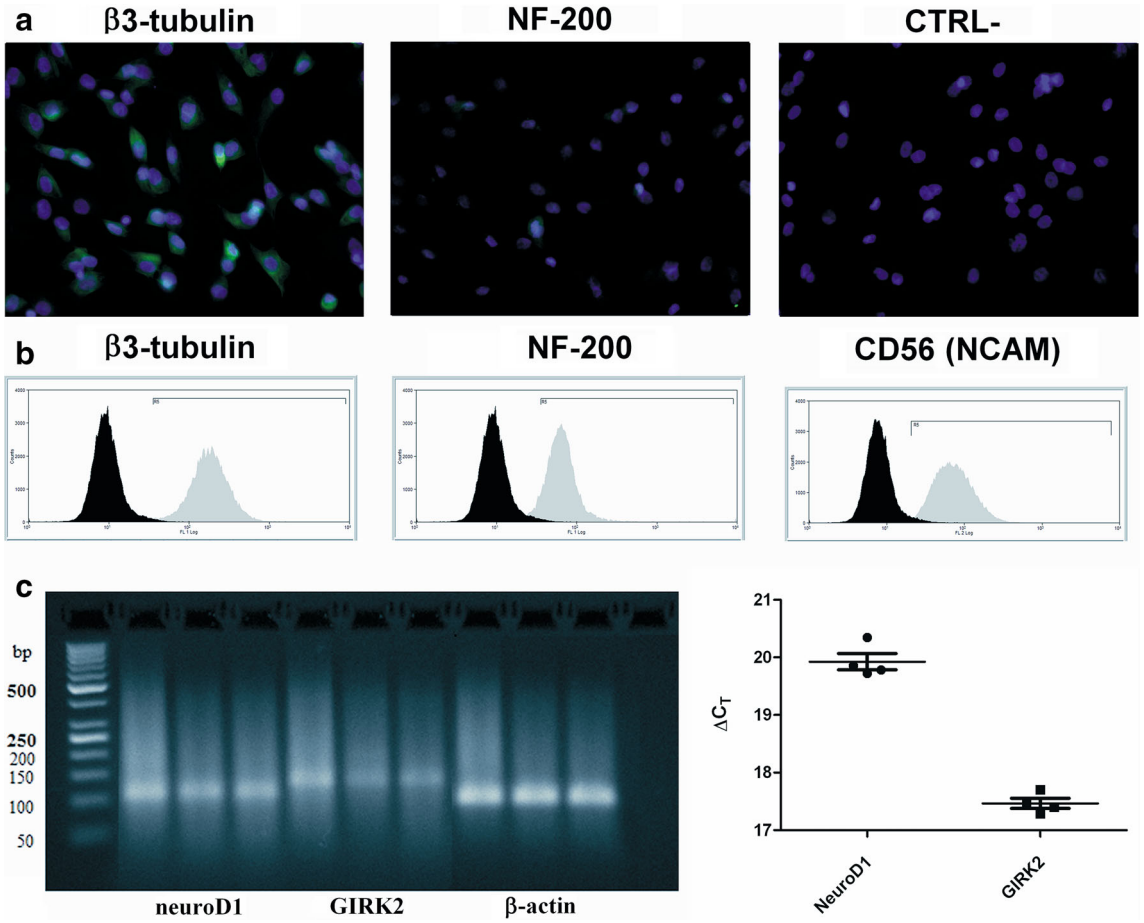

Fig. 5 Markers suggestive of neuronal progenitor commitment in cryopreserved AFSC. **a** Immunofluorescent staining (*green* AlexaFluor® 488, with *bright violet* DAPI nuclear counterstaining) for β3-tubulin, NF-200, and a negative control (CTRL-) lacking primary antibody. **b** Flow cytometry immunophenotyping for β3-tubulin, NF-200, and CD56/NCAM (distributions in *grey*) vs. negative control isotypes (distributions in *black*). **c** RT-PCR amplification products (agarose gel electrophoresis and ethidium bromide staining) for human neuroD1, GIRK2, and control gene β-actin; *last lane* represents a no-template control. *Right* relative quantitation of expression (SYBR® *Green* qPCR, ΔC_T relative to β-actin average) for the four replicates of neuroD1 and GIRK2 (individual values, mean ± SEM)

delayed rectifier K^+ channels ($I_{K\ DR}$) resulting from expression of genes hEAG1 and hEAG2 (human ether-à-go–go related gene), and big conductance Ca^{2+}-dependent K^+ channels (BK), giving current fluctuations at large depolarizing steps (over +40 mV), specifically blocked by iberiotoxin ($I_{K(Ca)}$ [21]. Further, via similar methods, the same group demonstrated differential increases in expression in induced pluripotent stem cells (iPSC) vs. ESC and MSC for ion channel subunits CACNA1H (Cav3.2), CACNA2D1 (Cav $\alpha_2\delta$-subunit1), CACNA2D2 (Cav $\alpha_2\delta$-subunit2), CACNG4 (Cav γ4-subunit), CACNG7 (Cav γ7-subunit), SCN8A (Nav1.6), KCNC4 (Kv3.4), KCNK1 (K_{2P}1.1), KCNK12 (K_{2P}12.1), KCNK5 (K_{2P}5.1), KCNK6 (K_{2P}6.1), KCNQ2 (Kv7.2), KCNS3 (Kv9.3), KCNMB4 (BK, subfamily M, β4), KCNN2 (K_{Ca}2.2), and HCN4 [22]. Despite increased gene expression, the only current that could be convincingly demonstrated via patch-clamp recordings in iPSC was a TEA-sensitive $I_{K\ DR}$ component, while $I_{K(Ca)}$, I_{Na}, I_{Ca}, and the hyperpolarization-activated (funny) current I_f, contributed by HCN (hyperpolarization-activated cyclic nucleotide-gated) channels, were completely absent.

A clue to the important functional roles of ion channels in stem cell development issued in the above-mentioned study was the fact that K^+ channel blocker TEA, and to a lesser extent 4-AP inhibited iPSC proliferation and viability when applied in the culture medium, with IC50 values in the low millimolar range, by arresting cells in the mitotic phase, as revealed by cell cycle analysis, while K(Ca) channel blockers iberiotoxin and apamin had no such effects. Another recent study of the same group demonstrates the important role of hEAG1K^+ channels in regulation of proliferation of iPSC and BM-MSC, via gene silencing with specific short hairpin interference RNA or

Table 2 Main types of ion currents identified in senescent and cryopreserved AFSC, numbers and percentages of cells where they were found, and mean current densities

Current	I_{or} outward rectifier	I_A inactivatable I_{or} component	BK-like current fluctuations	I_{Na}	$I_{K\ ir}$ inward rectifier
Senescent AFSC ($n = 18$)					
Number of cells	18	15	12	9	1
% of cells	100	83.33	66.67	50.00	5.56
Mean current density (pA/pF)	6.9	3.1	1.7	−2.8	−5.8
SD	8.0	2.7	1.5	3.0	–
Cryopreserved AFSC ($n = 19$)					
Number of cells	19	9	13	12	6
% of cells	100	47.37	68.42	63.16	31.58
Mean current density (pA/pF)	9.2	5.9	2.9	−13.1	−16.6
SD	9.1	8.5	2.4	23.7	24.9

Current densities were measured at +60 mV for I_{or}, I_A, and BK, at maximal peak amplitude (-10 or 0 mV) for I_{Na}, and at −120 mV for I_{Kir}

I_{or} outward rectifier current, I_A inactivatable (A-type) I_{or} current, I_{Na} voltage-dependent Na^+ current, I_{Kir} inward rectifier K^+ current

treatment with blocker 4-AP or astemizole [23]. A plausible explanation for this role of delayed rectifier K^+ channels would be related to the maintenance of a normal resting potential; when the K^+ channels are blocked or their expression is silenced, the resulting membrane depolarization activates Ca^{2+} channels, resulting in massive calcium entry followed by cell proliferation or cell death. An important insight in the molecular mechanisms that couple transmembrane potential to proliferation is the recent study of Zhou et al., who demonstrated that in depolarized cells phosphatidylserine and phosphatidylinositol (4,5) bisphosphate (PIP_2) nanoclustering results in K-Ras clustering with activation of the RAF-MAPK signaling cascade, promoting cell proliferation [24]. In the study of Zhang et al. [23], five ion current components were identified: $I_{K(Ca)}$ (BK), $I_{K\ DR}$, I_{Kir} (inward rectifier), non-BK $I_{K(Ca)}$, and chloride current I_{Cl}, present in 83, 47, 11, 5, and 4 % of iPSC-MSC, while in BM-MSC only four of them were present: $I_{K(Ca)}$ BK (76 %), $I_{K\ DR}$ (47 %), I_{Kir} (22 %), and $I_{K(Ca)}$ (non-BK) (11 %). These results are similar to our findings in AFSC, where we also identified five current components: I_{or} (persistent or sustained outward rectifier), I_A (A-type or inactivating component of outward rectifier current), $I_{K(Ca)}$(BK), I_{Na}, and I_{Kir}. The only currents that showed significant changes in expression between the two culture conditions were I_A, more prominent in senescent AFSC (83.3 vs. 47.4 %) and I_{Kir}, found almost exclusively in a subgroup of cryopreserved AFSC (31.6 vs. 5.6 %) (Table 2). Specific inhibition by paxilline of BK(Ca) channels in thoracic aorta smooth muscle was used as a test of successful grafting following intravenous administration of human MSC in non-fatal whole-body irradiated rats [25].

Actually, the discovery of a subset of cryopreserved AFSC presenting I_{Kir} together with high densities of I_{Na}, suggestive of neuronal differentiation (Fig. 4), was quite surprising. Similar surface densities of I_{Na} (10.15 vs. 13.1 pA/pF in our study), as well as the presence of inward-rectifying I–V plots (negative currents) were observed in rat bone marrow-derived mesenchymal stem cells cultured on neuronal layers [26]. Kir properties in our study, including the peculiar current–voltage relationship, time course, and mild inhibition by multivalent ions (we tested extracellular 100 μM RuR, although for a different reason), are similar to those described by De Coppi et al. for AFSC subjected to neuronal differentiation in vitro [13]. Their Kir current was slightly blocked by 200 μM extracellular Ba^{2+}, and by RT-PCR they identified it as result of expression of the GIRK2 gene. The increased density of I_{Na} during neuronal differentiation of human AFSC and the subsequent kinetic properties of TTX-sensitive voltage-dependent Na^+ channels have been also reported [27]. Other studies have also convincingly demonstrated the potential for neuronal or oligodendrocyte differentiation of AFSC [28], identifying neuronal morphology and markers such as tubulin β-III [29], but most of these markers were present even before induction [23] or before differentiation [30]. A possible explanation would be the paracrine secretion of BMP-4, a neural plate inductor, by nestin-positive mesenchymal stem cells present in the AFSC culture [31]. However, it will be difficult to understand whether dynamics of cell surface neuronal markers in in vitro conditions parallels the stages of human adult neuro/gliogenesis, which render remarkable plasticity to the mature brain [32].

Another interesting finding in our study was the progressive run-up of several current components, from very low initial levels, immediately after patch rupture and penetration in the whole-cell configuration, to considerably larger values, over an interval of a few minutes, in parallel

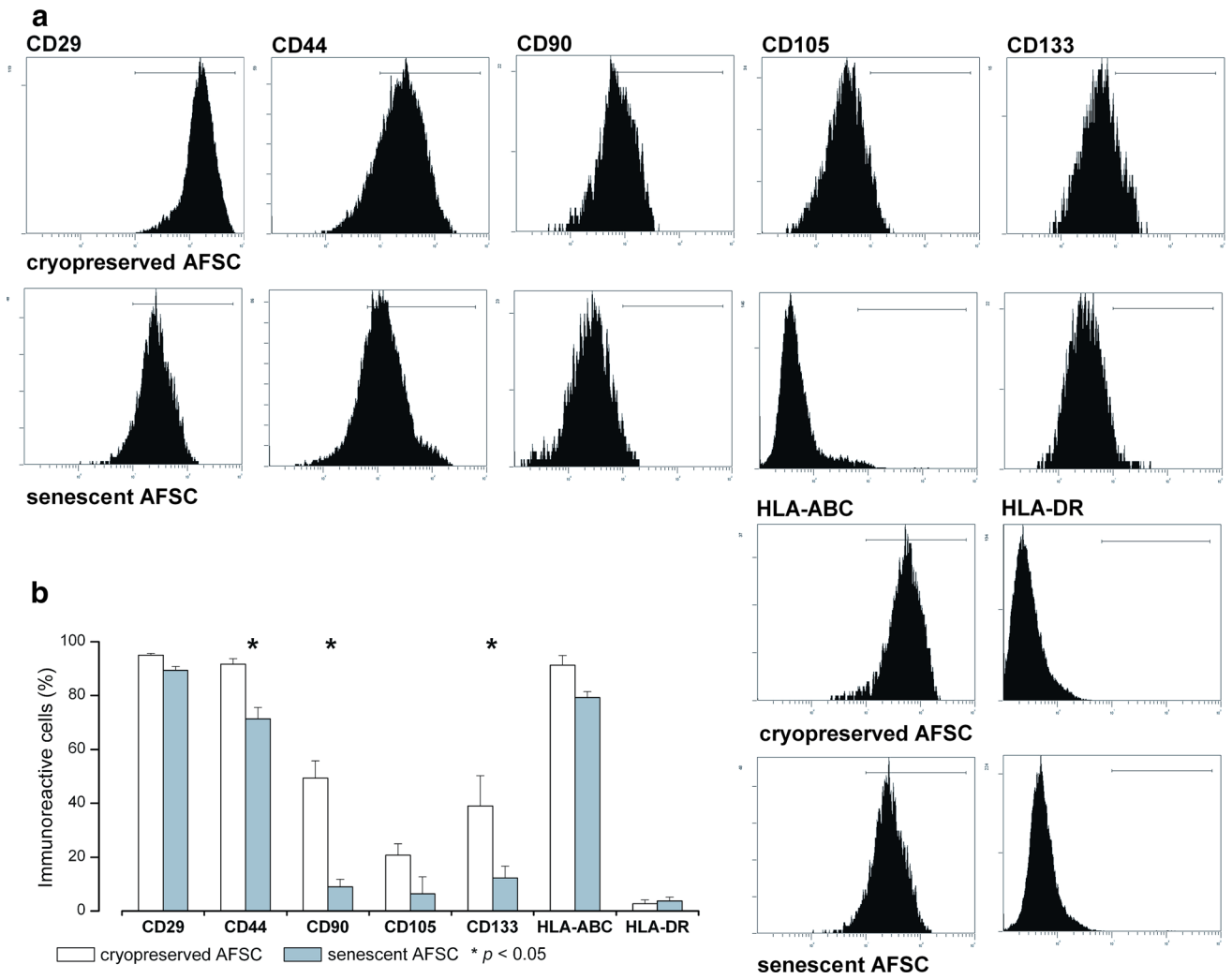

Fig. 6 Immunophenotype characterization of cryopreserved vs. senescent AFSC. *Asterisks* denote markers showing statistically significant differences between the two culture conditions ($p < 0.05$, one-way ANOVA)

to the dialysis of cytoplasm with pipette solution, as exemplified in Fig. 1. A plausible explanation for this behavior could be a phenomenon of secondary calcium release due to the relatively high concentration of chelator EGTA (5 mM) in the internal solution. Some K^+ channels, like BK(Ca), feature intrinsic sensitivity to intracellular calcium levels, while other K^+ channels could gain such features via interactions with proteins such as NCS-1 (neuronal calcium sensor-1). Recently, increased expression of calcium-sensing receptor (CaSR) in cultured AFSC and its role in osteogenic differentiation have been described [33].

Further issues currently lacking an adequate understanding are the changes in immunophenotype and gene expression associated with senescent AFSC. Recent reports describe the potential of transdifferentiation of AFSC in culture, and the autocrine modulatory effects of secreted growth factors like angiogenin, angiopoietin-1, endostatin/collagen XVIII, transforming growth factor β1 (TGFβ1), vascular endothelial growth factor (VEGF), FGF-7, serpin E1 and F1, urinary plasminogen activator (uPA), all responsible for tissue repair and regeneration, as well as differentiation factors insulin-like growth factor-binding proteins 2 and 3 (IGFBP-2 and 3) and tissue inhibitor of metalloproteinase 1 (TIMP-1) [34]. Other studies highlight the modulatory roles of microRNAs and non-coding RNAs, e.g., the inhibitory role of miR21 on Sox2 expression in spindle-shaped AFSC, resulting in reduced clonogenic and proliferative potential, cell cycle arrest, and induction of accelerated osteogenesis and impaired adipogenesis and chondrogenesis [35]. Another important factor modulating differentiation potential of mesenchymal stem cells is hypoxia-inducible factor 1α [36].

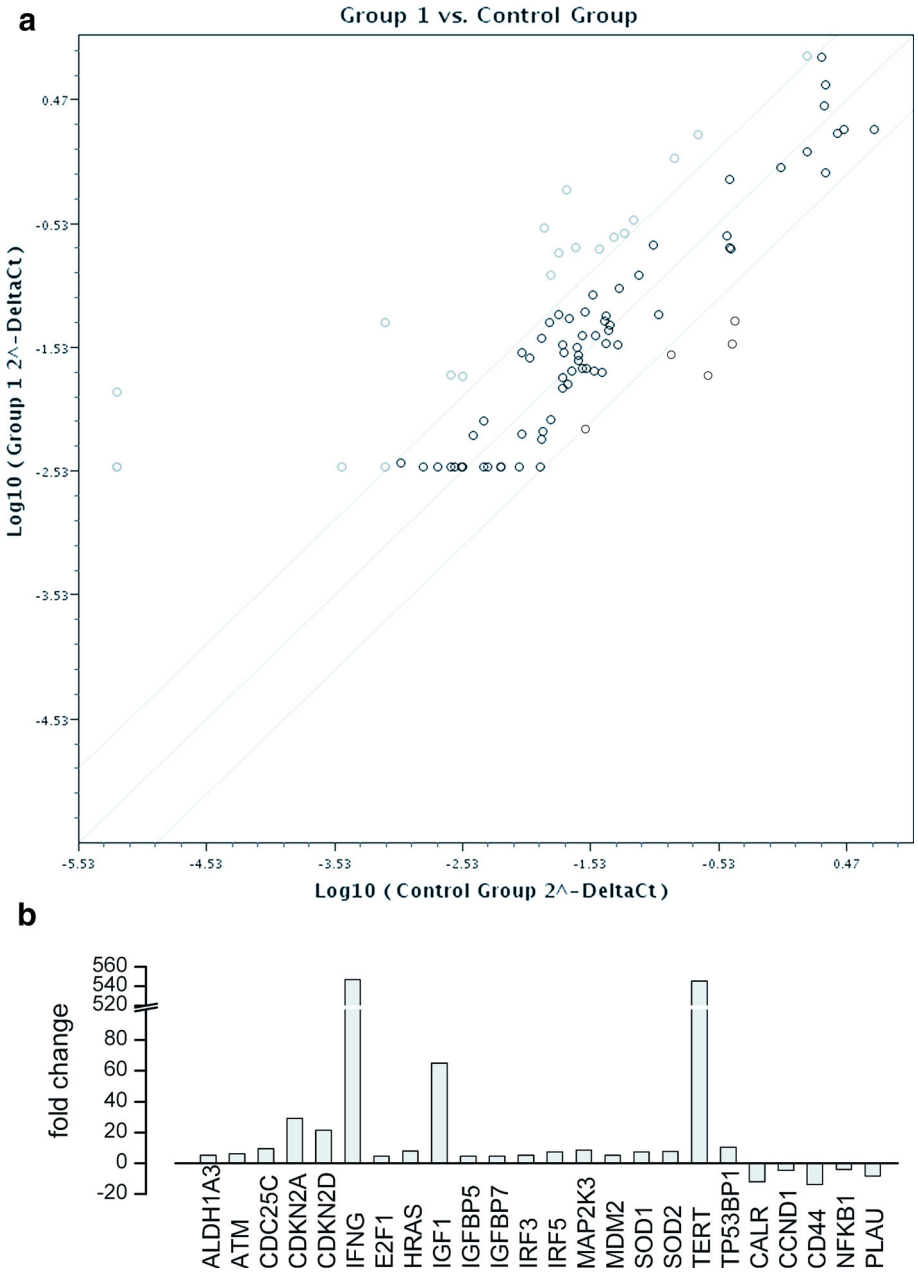

Fig. 7 **a** Differential gene expression profiling between senescent AFSC (6 weeks in vitro, group 1) and cryopreserved AFSC (control group) using the Human Cell Senescence RT^2 Profiler PCR Array (Qiagen). Genes with increased expression in senescent cells are *circled* with *thick gray lines*, those with preserved expression with *thick black lines*, and those with decreased expression with *thin black lines*. **b** Genes with overexpression or underexpression in senescent vs. cryopreserved AFSC

Conclusions

In conclusion, the complex regulatory networks activated during long-term culture of human AFSC, exerting major effects on phenotypic expression, proliferative, self-renewal and differentiation capacities, and therapeutically important properties of these cells including anti-inflammatory, tissue repair and regeneration, and antitumor potential, are currently not completely understood. Steady-state marker expression and functional properties of stem-cell-derived preparations is essential for artificial tissue engineering, but this type of homeostasis cannot be acquired in short-term (2–14 days) cultures [37]. In the present study, we have evidenced important changes in ion current surface densities, immunophenotype, and differential gene expression profile, in senescent human AFSC versus cryopreserved AFSC, but the underlying mechanisms and functional consequences await further exploration, requiring extensive research efforts.

Acknowledgments The authors gratefully acknowledge Adriana Georgescu and Violeta Ristoiu for instructive discussions, Antonia and Alexandru Deftu, Roxana-Olimpia Gheorghe, Cornelia Dragomir and Geanina Haralambie for technical assistance. This work was

supported from grants 1877/2014 "SORTIS" to Horia Maniu and PN2 80/2012 to Aurel Popa-Wagner.

Compliance with ethical standards

Conflict of interest The authors declare that they have no conflicts of interests related to this study.

References

1. Walker PA, Harting MT, Shah SK, Day MC, El Khoury R, Savitz SI, Baumgartner J, Cox CS (2010) Progenitor cell therapy for the treatment of central nervous system injury: a review of the state of current clinical trials. Stem Cells Int 2010:369578. doi:10.4061/2010/369578
2. Lipinski MJ, Biondi-Zoccai GG, Abbate A, Khianey R, Sheiban I, Bartunek J, Vanderheyden M, Kim HS, Kang HJ, Strauer BE, Vetrovec GW (2007) Impact of intracoronary cell therapy on left ventricular function in the setting of acute myocardial infarction: a collaborative systematic review and meta-analysis of controlled clinical trials. J Am Coll Cardiol 50:1761–1767
3. Kang NH, Hwang KA, Kim SU, Kim YB, Hyun SH, Jeung EB, Choi KC (2012) Potential antitumor therapeutic strategies of human amniotic membrane and amniotic fluid-derived stem cells. Cancer Gene Ther 19:517–522
4. Koç ON, Gerson SL, Cooper BW, Dyhouse SM, Haynesworth SE, Caplan AI, Lazarus HM (2000) Rapid hematopoietic recovery after coinfusion of autologous-blood stem cells and culture-expanded marrow mesenchymal stem cells in advanced breast cancer patients receiving high-dose chemotherapy. J Clin Oncol 18:307–316
5. Petite H, Viateau V, Bensaïd W, Meunier A, de Pollak C, Bourguignon M, Oudina K, Sedel L, Guillemin G (2000) Tissue-engineered bone regeneration. Nat Biotechnol 18:959–963
6. Baksh D, Song L, Tuan RS (2004) Adult mesenchymal stem cells: characterization, differentiation, and application in cell and gene therapy. J Cell Mol Med 8:301–316
7. Zhou J, Wang D, Liang T, Guo Q, Zhang G (2014) Amniotic fluid-derived mesenchymal stem cells: characteristics and therapeutic applications. Arch Gynecol Obstet 290:223–231
8. Dobreva MP, Pereira PN, Deprest J, Zwijsen A (2010) On the origin of amniotic stem cells: of mice and men. Int J Dev Biol 54:761–777
9. Cananzi M, De Coppi P (2012) CD117(+) amniotic fluid stem cells: state of the art and future perspectives. Organogenesis 8:77–88
10. Zhang S, Geng H, Xie H, Wu Q, Ma X, Zhou J, Chen F (2010) The heterogeneity of cell subtypes from a primary culture of human amniotic fluid. Cell Mol Biol Lett 15:424–439
11. Maguire CT, Demarest BL, Hill JT, Palmer JD, Brothman AR, Yost HJ, Condic ML (2013) Genome-wide analysis reveals the unique stem cell identity of human amniocytes. PLoS One 8:e53372
12. Sousa BR, Parreira RC, Fonseca EA, Amaya MJ, Tonelli FM, Lacerda SM, Lalwani P, Santos AK, Gomes KN, Ulrich H, Kihara AH, Resende RR (2014) Human adult stem cells from diverse origins: an overview from multiparametric immunophenotyping to clinical applications. Cytometry A 85:43–77
13. De Coppi P, Bartsch G Jr, Siddiqui MM, Xu T, Santos CC, Perin L, Mostoslavsky G, Serre AC, Snyder EY, Yoo JJ, Furth ME, Soker S, Atala A (2007) Isolation of amniotic stem cell lines with potential for therapy. Nat Biotechnol 25:100–106
14. Bai J, Wang Y, Liu L, Chen J, Yang W, Gao L, Wang Y (2012) Human amniotic fluid-derived c-kit (+) and c-kit (−) stem cells: growth characteristics and some differentiation potential capacities comparison. Cytotechnology 64:577–589
15. Katoh M (2011) Network of WNT and other regulatory signaling cascades in pluripotent stem cells and cancer stem cells. Curr Pharm Biotechnol 12:160–170
16. Xu RH, Sampsell-Barron TL, Gu F, Root S, Peck RM, Pan G, Yu J, Antosiewicz-Bourget J, Tian S, Stewart R, Thomson JA (2008) NANOG is a direct target of TGFbeta/activin-mediated SMAD signaling in human ESCs. Cell Stem Cell 3:196–206
17. Amendola D, Nardella M, Guglielmi L, Cerquetti L, Carico E, Alesi V, Porru M, Leonetti C, Bearzi C, Rizzi R, D'Agnano I, Stigliano A, Novelli G, Bucci B (2014). Human placenta-derived neurospheres are susceptible to transformation after extensive in vitro expansion. Stem Cell Res Ther 5
18. Lu Q, Gong L, Xu H, Zhang T, Yan X, Zhao J, Zhang Z, Wang Y, Han Y (2011) Identification of GIRK2-4 subunits in human esophageal smooth muscle cells. Mol Med Rep 4:941–945. doi:10.3892/mmr.2011.3499 **Epub 2011 May 3831**
19. An WF, Bowlby MR, Betty M, Cao J, Ling HP, Mendoza G, Hinson JW, Mattsson KI, Strassle BW, Trimmer JS, Rhodes KJ (2000) Modulation of A-type potassium channels by a family of calcium sensors. Nature 403:553–556
20. Van Driessche W, Zeiske W (1980) Spontaneous fluctuations of potassium channels in the apical membrane of frog skin. J Physiol 299:101–116
21. Li GR, Sun H, Deng X, Lau CP (2005) Characterization of ionic currents in human mesenchymal stem cells from bone marrow. Stem Cells 23:371–382
22. Jiang P, Rushing SN, Kong CW, Fu J, Lieu DK, Chan CW, Deng W, Li RA (2010) Electrophysiological properties of human induced pluripotent stem cells. Am J Physiol Cell Physiol 298:C486–C495
23. Zhang J, Chan YC, Ho JC, Siu CW, Lian Q, Tse HF (2012) Regulation of cell proliferation of human induced pluripotent stem cell-derived mesenchymal stem cells via ether-a-go-go 1 (hEAG1) potassium channel. Am J Physiol Cell Physiol 303:C115–C125
24. Zhou Y, Wong CO, Cho KJ, van der Hoeven D, Liang H, Thakur DP, Luo J, Babic M, Zinsmaier KE, Zhu MX, Hu H, Venkatachalam K, Hancock JF (2015) SIGNAL TRANSDUCTION. Membrane potential modulates plasma membrane phospholipid dynamics and K-Ras signaling. Science 349:873–876
25. Soloviev A, Prudnikov I, Tsyvkin V, Tishkin S, Kyrychenko S, Zelensky S, Ivanova I (2010) Electrophysiological and contractile evidence of the ability of human mesenchymal stromal cells to correct vascular malfunction in rats after ionizing irradiation. J Physiol Sci 60:161–172
26. Wislet-Gendebien S, Hans G, Leprince P, Rigo JM, Moonen G, Rogister B (2005) Plasticity of cultured mesenchymal stem cells: switch from nestin-positive to excitable neuron-like phenotype. Stem Cells 23:392–402
27. Mareschi K, Rustichelli D, Comunanza V, De Fazio R, Cravero C, Morterra G, Martinoglio B, Medico E, Carbone E, Benedetto C, Fagioli F (2009) Multipotent mesenchymal stem cells from amniotic fluid originate neural precursors with functional voltage-gated sodium channels. Cytotherapy 11:534–547
28. Maraldi T, Bertoni L, Riccio M, Zavatti M, Carnevale G, Resca E, Guida M, Beretti F, La Sala GB, De Pol A (2014) Human amniotic fluid stem cells: neural differentiation in vitro and in vivo. Cell Tissue Res 357:1–13
29. Tsai MS, Lee JL, Chang YJ, Hwang SM (2004) Isolation of human multipotent mesenchymal stem cells from second-trimester amniotic fluid using a novel two-stage culture protocol. Hum Reprod 19:1450–1456 **Epub 2004 Apr 1422**
30. Tsai MS, Hwang SM, Tsai YL, Cheng FC, Lee JL, Chang YJ (2006) Clonal amniotic fluid-derived stem cells express

characteristics of both mesenchymal and neural stem cells. Biol Reprod 74:545–551 **Epub 2005 Nov 2023**
31. Wislet-Gendebien S, Bruyère F, Hans G, Leprince P, Moonen G, Rogister B (2004) Nestin-positive mesenchymal stem cells favour the astroglial lineage in neural progenitors and stem cells by releasing active BMP4. BMC Neurosci 5:33
32. Yamaguchi M, Seki T, Imayoshi I, Tamamaki N, Hayashi Y, Tatebayashi Y, Hitoshi S (2015). Neural stem cells and neuro/gliogenesis in the central nervous system: understanding the structural and functional plasticity of the developing, mature, and diseased brain. J Physiol Sci. Epub ahead of print 2015 Nov 17
33. Di Tomo P, Pipino C, Lanuti P, Morabito C, Pierdomenico L, Sirolli V, Bonomini M, Miscia S, Mariggio MA, Marchisio M, Barboni B, Pandolfi A (2013) Calcium sensing receptor expression in ovine amniotic fluid mesenchymal stem cells and the potential role of R-568 during osteogenic differentiation. PLoS One 8:e73816
34. Zagoura DS, Trohatou O, Bitsika V, Makridakis M, Pappa KI, Vlahou A, Roubelakis MG, Anagnou NP (2013) AF-MSCs fate can be regulated by culture conditions. Cell Death Dis 4:e571
35. Trohatou O, Zagoura D, Bitsika V, Pappa KI, Antsaklis A, Anagnou NP, Roubelakis MG (2014) Sox2 suppression by miR-21 governs human mesenchymal stem cell properties. Stem Cells Transl Med 3:54–68
36. Wang Y, Feng C, Xue J, Sun A, Li J, Wu J (2009) Adenovirus-mediated hypoxia-inducible factor 1alpha double-mutant promotes differentiation of bone marrow stem cells to cardiomyocytes. J Physiol Sci 59:413–420. doi:10.1007/s12576-12009-10050-x **Epub 12009 Jul 12515**
37. Abbott RD, Kaplan DL (2015) Strategies for improving the physiological relevance of human engineered tissues. Trends Biotechnol 33:401–407